Article

On the Effective Charge of Hydrophobic Polyelectrolytes

A. Chepelianskii, F. Mohammad-Rafiee, E. Trizac, and E. Raphae#l

More About This Article

Additional resources and features associated with this article are available within the HTML version:

- Supporting Information
- Access to high resolution figures
- Links to articles and content related to this article
- Copyright permission to reproduce figures and/or text from this article

View the Full Text HTML

On the Effective Charge of Hydrophobic Polyelectrolytes[†]

A. Chepelianskii,[‡] F. Mohammad-Rafiee,[§,⊥] E. Trizac,[#] and E. Raphaël*,[⊥]

Laboratoire de Physique des Solides, UMR CNRS 8502, Bat. 510, Université Paris-Sud, 91405 Orsay, France, Institute for Advanced Studies in Basic Sciences (IASBS), Zanjan 45195, P.O. Box 45195-1159, Iran, Laboratoire Physico-Chimie Théorique, UMR CNRS Gulliver 7083, ESPCI, 10 rue Vauquelin, 75005 Paris, France, and Université Paris-Sud, LPTMS, UMR CNRS 8626, 91405 Orsay, France

In this paper, we analyze the behavior of hydrophobic polyelectrolytes. It has been proposed that this system adopts a pearl necklace structure reminiscent of the Rayleigh instability of a charged droplet. Using a Poisson–Boltzmann approach, we calculate the counterion distribution around a given pearl, assuming the latter to be penetrable for the counterions. This allows us to calculate the effective electric charge of the pearl as a function of the chemical charge. Our predictions are in good agreement with the recent experimental measurements of the effective charge by Essafi et al. (Essafi, W.; Lafuma, F.; Baigl, D.; Williams, C. E. *Europhys. Lett.* 2005, *71*, 938.). Our results allow us to understand the large deviation from the Manning law observed in these experiments.

I. Introduction

The study of polyelectrolytes has attracted an increased attention in the scientific community over the last decades. This interest is motivated by technological applications including viscosity modifiers, or leak protectors, and by the hope that advances in this domain will allow to unravel the structure of complex biological macromolecules. In these systems, the Coulomb interactions leads to many remarkable and counter-intuitive phenomena.[1–5] A celebrated example is the Manning–Oosawa counterion condensation. In his classical work,[1] Manning showed that a charged rod-like polymer can create such a strong attractive force on its counterions that a finite fraction condenses onto the polymer backbone. This condensation phenomenon was also described by Oosawa within a two-state model.[2] It leads to an effective decrease of the polymer charge, and the macroscopic properties of the polyelectrolyte, like migration in an electrophoresis experiment, are not determined by its bare charge but by an effective charge that accounts for the Manning–Oosawa counterion condensation. It is now well-established that counterion condensation is a fundamental phenomenon and that it occurs in many important systems including DNA in both its double-stranded and single-stranded form.[6] It was predicted in ref 1 that condensation occurs whenever the average distance l between co-ions (assumed here to be monovalent) on the polymer backbone is smaller than the Bjerrum length $l_B = q^2/(4\pi\epsilon\epsilon_0 k_B T)$, where q is the elementary charge, $k_B T$ the thermal energy, and ϵ the (relative) dielectric constant of the solvent. This condensation is expected to lead to an average charge density of q/l_B on the polymer backbone. Since the original prediction by Manning, important efforts have been devoted to a description of the Manning–Oosawa condensation within the Poisson–Boltzmann theory and beyond,[7–11]

establishing the influence of salt, the thickness of the condensed counterion layer, and the corrections induced by short-range correlation.

While the conformation of many polyelectrolytes is well described by the rod-like model, many proteins organize into complex self-assembled structures.[12] A challenging and important topic is the extent to which the structural complexity of biological enzymes can be understood from simple physical models. Polyelectrolytes with a hydrophobic backbone may provide an interesting system that achieves a certain degree of self-organization while the relevant interactions remain relatively simple. Indeed, it has been predicted in a seminal paper by Dobrynin and Rubinstein that hydrophobic polyelectrolytes should fold into an organized pearl necklace structure where regions of high and low monomer density coexist.[13] Therefore, both theoretical and experimental studies of the hydrophobic polyelectrolytes have shown a growing activity in the past few years.[4,5,14–21]

The question of the validity of the Manning condensation model for hydrophobic polyelectrolytes has been addressed experimentally by W. Essafi et al.[22] The authors have measured the effective charge fraction of a highly charged hydrophobic polyelectrolyte (poly(styrene)-co-styrene sulfonate) by osmotic pressure and cryoscopy measurements. Their findings, which are recalled in Figure 4, showed that the measured effective charge is significantly smaller than that predicted by the Manning–Oosawa theory. The aim of the present article is to provide a theoretical explanation of the counterion condensation in this system, where the hydrophobicity of the backbone strongly influences its conformation. This problem was first addressed theoretically by Dobrynin and Rubinstein,[17] who analyzed the phase diagram of a solution of hydrophobic polyelectrolytes as a function of solvent quality and polymer concentration. However, the question of the effective charge of the chains was not directly investigated by the authors.

The rest of the paper is organized as follows. In section II, the pearl necklace model is reviewed briefly, while the Poisson–Boltzmann theory of a hydrophobic globule permeable to counterions is performed in section III. The resulting effective

charge is analyzed in section IV. Some aspects of the model are discussed in section V, and finally, section VI concludes the paper.

II. Review of the Pearl Necklace Model

Let us first recall, for completeness, the pearl necklace theory of hydrophobic polyelectrolytes (for a more complete review, see ref 21). The polyelectrolyte solution is parametrized by its degree of polymerization N, its monomer size b (for the polyelectrolytes used by W. Essafi et. al, one has $b \approx 0.25$ nm), the charge fraction along the chain f, and the reduced temperature $\tau \equiv 1 - \Theta/T$, where Θ and T denote the theta temperature of the polyelectrolyte and the temperature of the system, respectively. We note that in a bad solvent, the reduced temperature is negative $\tau < 0$. Let us denote by C the average monomer concentration in the solution.

In a poor solvent, an uncharged polymer forms a globule in order to decrease its surface energy. In a similar way, a drop of water adopts a spherical configuration in a hydrophobic environment.

To estimate the gyration radius R_g of the polymer, we divide the polymer into smaller units, in such a way that inside of each unit, the thermal fluctuations dominate and the chain has Gaussian behavior. These units are usually called thermal blobs in the literature, and the typical radius of the blobs is denoted by ξ_T. It can be shown that they contain about $1/\tau^2$ monomers and have a typical size of $\xi_T \simeq b/|\tau|$. At larger scales, the polymer tends to collapse onto itself in order to minimize its surface of contact with the liquid. This can happen by forming a dense packing of thermal blobs. A polymer of polymerization degree N can be split into $\tau^2 N$ thermal blobs, and the volume occupied by the polymer is proportional to the number of subunits. Therefore, one can estimate the gyration radius of the polymer as

$$R_g^3 \simeq \tau^2 N \xi_T^3 \simeq \frac{Nb^3}{|\tau|} \qquad (1)$$

The surface energy E_S associated with this configuration is given by $k_B T$ times the number of thermal blobs in contact with the solvent. This leads to

$$\frac{E_S}{k_B T} \simeq \frac{\tau^2 R_g^2}{b^2} \qquad (2)$$

Upon charging, the electrostatic repulsion sets in, which results in a change of the globule shape. When the electrostatic repulsion energy becomes larger than the surface energy, the globule splits into several globules of smaller size consisting of N_g monomers. According to eq 1, the typical size of these globules is given by

$$R_g^3 \simeq \frac{N_g b^3}{|\tau|} \qquad (3)$$

This behavior is reminiscent of the Rayleigh instability of a charged droplet.[23] In this state, the polyelectrolyte forms a sequence of globules that are connected by strings made of thermal blobs (see Figure 1). In the literature, this conformation is known as the "pearl necklace" structure. The presence of counterions will screen the electrostatic repulsion. Therefore,
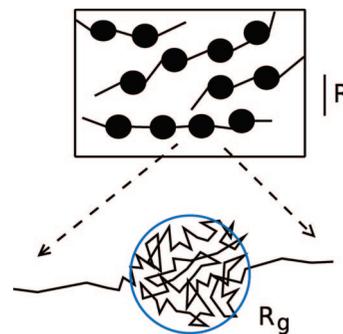

Figure 1. Schematic drawing of the pearl necklace structure of hydrophobic polyelectrolytes. Inside of the blue (gray) circle, the polymer backbone, represented by a continuous black line, is wrapped into a dense configuration of typical radius R_g, which we call pearl or globule in the text. The inset shows on a larger scale that these pearls are connected by thin polymer strings, thus forming the pearl necklace structure. The average distance between the pearls is R (black vertical scale line).

it is important to account for their role explicitly in the balance between the surface tension and the electrostatic repulsion that governs the equilibrium structure of the necklace.

For simplicity, we assume that the main effect of the counterions is to reduce the charge of the pearls. Indeed, some counterions can be attracted inside of the globules due to the attractive electrostatic forces. In the absence of any counterion condensation, the total electrostatic charge of a globule consisting of N_g monomers is simply given by qfN_g. (where q is the elementary charge). If the (monovalent) counterions penetrate inside the globule, its effective charge is decreased and is given by $qf_{eff}N_g$, where f_{eff} denotes the effective charge fraction. We can understand this relation by noting that in the presence of counterion condensation, the total charge of the pearl is the chemical charge of the pearl minus the charge of the counterions inside of it. Therefore, the electrostatic energy E_{el} of a pearl can be estimated as

$$\frac{E_{el}}{k_B T} \simeq \frac{l_B (f_{eff} N_g)^2}{R_g} \qquad (4)$$

where the Bjerrum length is defined as

$$l_B = \frac{q^2}{4\pi\epsilon\epsilon_0 k_B T} \qquad (5)$$

where ϵ is the dielectric constant of the medium and $k_B T$ denotes the thermal fluctuation energy. For example, for water at room temperature ($T = 300$ K, $\epsilon = 80$), the value of the Bjerrum length is $l_B \approx 0.7$ nm. Using the relation between R_g and the N_g given in eq 3, the electrostatic energy of a pearl is simplified to

$$\frac{E_{el}}{k_B T} \simeq |\tau|^2 f_{eff}^2 \frac{l_B R_g^5}{b^6} \qquad (6)$$

In its equilibrium configuration the pearl necklace tends to balance its electrostatic and surface energies $E_{el} \simeq E_S$. Inserting the results of eqs 2 and 6 into this equality leads to an expression of the globule radius R_g as a function of the effective charge fraction f_{eff}

On the Effective Charge of Hydrophobic Polyelectrolytes

J. Phys. Chem. B, Vol. 113, No. 12, 2009 **3745**

$$R_g \simeq b\left(\frac{b}{l_B}\right)^{1/3}\frac{1}{f_{eff}^{2/3}} \tag{7}$$

We stress that this relation between the typical pearl size and the effective charge has been verified experimentally by D. Baigl et al. in ref 24 with an X-ray diffraction technique. This suggests that the hydrophobic polyelectrolytes studied in the experiment of W. Essafi actually formed a pearl necklace structure.

III. Screening of a Globule in the Poisson−Boltzmann Theory

The problem of the effective charge of spherical microion-permeable globules of size R_g surrounded by their own counterions can be solved in the mean-field approximation using the Poisson−Boltzmann theory. This problem was first studied numerically and analytically by Wall and Berkowitz.[25] It was shown that for such a globule, counterion condensation can occur (see, e.g., ref 26 for a general discussion of the condensation phenomenon). In this approach, a charged globule is modeled as a sphere with radius R_g and a uniform charge distribution inside of it. Therefore, the charge density of the globule is given by

$$q\rho_0 \simeq q\frac{fN_g}{R_g^3} \tag{8}$$

where ρ_0 denotes the mean density of charged monomers that are distributed inside of the globule. Using eq 3, ρ_0 can be simplified to

$$\rho_0 \simeq \frac{f|\tau|}{b^3} \tag{9}$$

In the solution, the mean monomer concentration is denoted by C. As far as the counterions are distributed inside of an elementary cell of radius R (Wigner−Seitz approach), the average concentration of the counterions is given by

$$n_{av} = fC \tag{10}$$

Using the electroneutrality condition, one can find a relation between the radius of the elementary cell, R, and the density of the charged monomers inside of the globule as

$$\rho_0 R_g^3 = n_{av}R^3 \tag{11}$$

Assuming a spherical symmetry for the charge distribution, all of the quantities such as the electrostatic potential, the counterion concentration, and so forth depend only on the distance r to the center of the globule. Under the assumption of a Boltzmann distribution, the concentration profile $n(r)$ of the counterions is related to the electrostatic potential $\phi(r)$ as

$$n(r) = n_{av}e^{q\phi(r)/k_BT} \tag{12}$$

Inserting this expression into the Poisson equation $\nabla^2\phi = -(1/\epsilon\epsilon_0)(q\rho_0(r) - qn(r))$ leads to the well-known Poisson−Boltzmann (PB) equation

$$\nabla^2\phi = \frac{1}{r^2}\frac{d}{dr}\left(r^2\frac{d\phi}{dr}\right) = -\frac{q\rho_0(r)}{\epsilon\epsilon_0} + \frac{qn_{av}}{\epsilon\epsilon_0}e^{q\phi/k_BT} \tag{13}$$

where $\rho_0(r)$ is given by

$$\rho_0(r) = \begin{cases} \rho_0 \simeq \dfrac{fN_g}{R_g^3} & r \leq R_g \\ 0 & r > R_g \end{cases} \tag{14}$$

For our system with spherical symmetry in the charge distribution, the electric field is zero at $r = 0$. Electroneutrality also demands a vanishing electric field at the boundary $r = R$, so that the boundary conditions for the above PB equation read

$$\frac{d\phi(r = 0)}{dr} = \frac{d\phi(r = R)}{dr} = 0 \tag{15}$$

In an elementary cell with the average counterion density n_{av}, the Debye screening length λ_D is given by

$$\frac{1}{\lambda_D^2} = 4\pi l_B n_{av} \tag{16}$$

After defining the reduced electrostatic potential, $u \equiv q\phi/(k_BT)$, and $x \equiv r/\lambda_D$, the PB equation can be written as

$$\frac{d^2u}{dx^2} + \frac{2}{x}\frac{du}{dx} = e^{u(x)} - A(x) \qquad \frac{du(0)}{dx} = \frac{du(X)}{dx} = 0 \tag{17}$$

where X denotes R/λ_D and $A(x)$ is defined as

$$A(x) \equiv \frac{\rho_0(x)}{n_{av}} \tag{18}$$

The radius of the globule in the dimensionless form is denoted by $x_g \equiv R_g/\lambda_D$. We will set A as the value of $A(x)$ inside of the globule, $A(x) = A$ for $x \leq x_g$. Using the aforementioned reduced variables and the cell neutrality condition, eq 11, one can find the simple form of A as

$$A = \frac{\rho_0}{n_{av}} = \left(\frac{X}{x_g}\right)^3 \simeq \frac{|\tau|}{Cb^3} \tag{19}$$

where, in writing the last term, the explicit forms of ρ_0, eq 9, and n_{av}, eq 10, have been used. It appears that A does not depend on the chemical charge f. The quantity A may be seen as the inverse packing (or volume) fraction.

The fraction of counterions outside of the globule, P, can be found as

$$P = \frac{\int_{r_g}^R n_{av}e^{q\phi(r)/k_BT}r^2dr}{\int_0^{R_g}\rho_0 r^2dr} = \frac{\int_{x_g}^X e^u x^2dx}{\int_0^{x_g}Ax^2dx} \tag{20}$$

where, in writing the last term, the reduced variables and eq 19 have been used. Using eq 17, integration leads to a simpler form of the above equation

$$P(x_g, A) = -\frac{3}{x_g A}\frac{du(x_g)}{dx} \tag{21}$$

As far as the penetrated counterions inside of the globule reduce its charge, the effective charge of the globule is proportional to the fraction of counterions outside of the globule. Therefore, the effective charge of the globule can be written as

$$f_{eff} = P(x_g, A)f \tag{22}$$

It has been shown in ref 25 that the potential $u(x)$ defined by the boundary problem, eq 17, is a decreasing function of x, and the initial value of the potential satisfies $e^{u(0)} \leq A$. Physically, this inequality signifies the absence of overscreening (inside of the globule, $qn(r) \leq \rho_0$) as expected in mean-field theory.[27] In order to estimate the lower limit of $e^{u(0)}$, we rewrite eq 17 as

$$u(x) = u(0) + \int_0^x \left(y - \frac{y^2}{x}\right)[e^{u(y)} - A(y)]dy \tag{23}$$

Since $u(x)$ is a decreasing function, it may be shown that

$$u(x) = u(0) + \frac{1}{6}\min(x, x_g)^2[e^{u(0)} - A] \tag{24}$$

where min (x, x_g) yields the smallest quantity. After inserting this result into the cell neutrality condition, $\int_0^X x^2[e^{u(x)} - A(x)]dx$, we find that $e^{u(0)}$ satisfies the following inequality relations

$$1 - 2\frac{\ln(\tilde{Z}_g/2)}{\tilde{Z}_g} \leq \frac{e^{u(0)}}{A} \leq 1 \tag{25}$$

where we have set $\tilde{Z}_g = Ax_g^2/3 > e$. The quantity $\tilde{Z}_g$ has a simple interpretation as the total charge of the co-ions inside of the globule $Z_g = (4\pi/3)\rho_0 R_g^3$ multiplied by the ratio between the Bjerrum length and the globule radius l_B/R_g. Indeed, the following equality

$$\tilde{Z}_g \equiv Z_g\frac{l_B}{R_g} = \frac{1}{3}x_g^2 A \tag{26}$$

can be checked using the relations $R_g = x_g\lambda_D$, $\rho_0 = n_{av}A$, and the expression of the Debye length λ_D from eq 16. In what follows, we will refer to $\tilde{Z}_g$ as the reduced globule charge. With these notations, the chain of inequalities in eq 25 implies that in the limit of large reduced globule charge $\tilde{Z}_g \gg 1$, we have $e^{u(0)}/A \to 1$.

The behavior of a typical solution $u(x)$ is displayed in Figure 2. It confirms that for large values of $\tilde{Z}_g$, the counterion concentration at $x \simeq 0$ is very close to the concentration of charged monomers inside of the globule, $e^{u(x)} \simeq A$. As the value of $\tilde{Z}_g$ increases, the size of the neutral region where $u(x) \approx \ln A$ grows until it becomes on the order of globule size x_g.
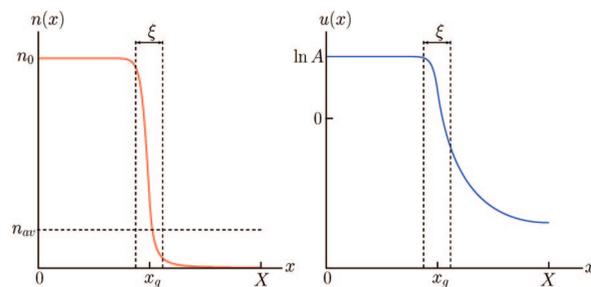

Figure 2. Typical behavior of counterion charge distribution $n(x)$ and effective potential $u(x)$ in the cell. The dimensionless globule size is denoted by x_g, and the cell size is denoted by X. The n_0 corresponds to $n(x = 0)$ and is very close to ρ_0 (the mean density of charged monomers that are distributed inside of the globule; see eq 9). At large x, $n(x)$ tends to a (exponentially small) constant, as can be inferred from the large x behavior of $u(x)$.

Therefore, to keep the system electrically neutral, the counterion concentration must fall down to values below n_{av} outside of the globule.

The transition between these two regions occurs in a narrow layer of thickness ξ on the boundary of the globule, as shown in Figure 2. In order to estimate the behavior of ξ in terms of the physical parameters of the problem, it is convenient to write the PB equation for $x \gtrsim x_g$ in the following manner

$$\frac{d^2u}{dx^2}\left[1 + \frac{2}{x}\frac{du/dx}{d^2u/dx^2}\right] = e^{u(x)} \tag{27}$$

We note that d^2u/dx^2 and du/dx are on the order of $(\ln A)/\xi^2$ and $(\ln A)/\xi$, respectively. Putting these values in the above equation, we find

$$\frac{\ln A}{\xi^2}\left[1 + 2\frac{\xi}{x_g}\right] \simeq A \tag{28}$$

We assume that we are in the regime where $\xi/x_g \ll 1$. Therefore, ξ scales as

$$\frac{\ln A}{\xi^2} \simeq A \Rightarrow \xi \simeq \frac{1}{\sqrt{A}} \tag{29}$$

where we have neglected the logarithmic dependence on A. We note that, for consistency, the requirement $\xi \ll x_g$ also implies $\tilde{Z}_g \gg 1$.

We are now in a position to estimate the counterion concentration outside of the globule. Using eq 21 in the limit of $\tilde{Z}_g \gg 1$, the fraction of counterions outside of the globule is found as

$$P(x_g, A) \simeq \frac{1}{x_g A}\frac{u}{\xi} \simeq \frac{6}{\sqrt{2e}}\frac{1}{x_g\sqrt{A}} \tag{30}$$

Using eq 26, we find that in the asymptotic regime of $\tilde{Z}_g \gg 1$, P depends only on the reduced globule charge $\tilde{Z}_g$ through the simple equation

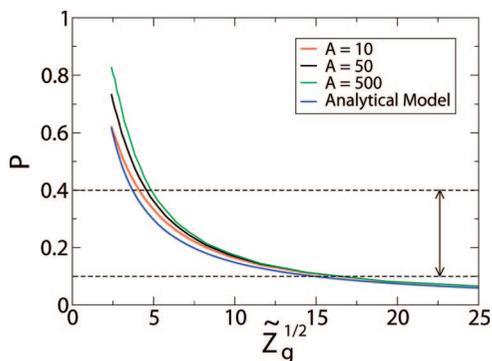$$P = \sqrt{\frac{6}{e\tilde{Z}_g}} \tag{31}$$

On the Effective Charge of Hydrophobic Polyelectrolytes

J. Phys. Chem. B, Vol. 113, No. 12, 2009 **3747**

Figure 3. Dependence of P on $\tilde{Z}_g^{1/2}$ for different values of A. From top to bottom, $A = 500, 50,$ and 10 (green, black, and red curves, respectively), where A is the inverse volume fraction of the globules. The bottom (blue) curve is eq 30. The arrow shows the P range explored in the experiment. It is obtained by calculating the ratio f_{eff}/f from the experimental data in Figure 4.
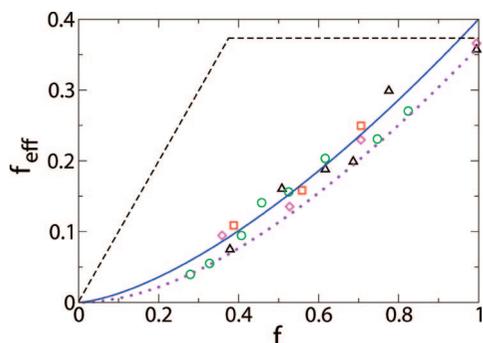

Figure 4. Effective charge fraction f_{eff} versus the chemical charge fraction f. The experimental points were obtained in ref 22. The red squares correspond to $N = 410$, green circles to $N = 930$, purple diamonds to $N = 1320$, and black deltas to $N = 2400$. The blue solid line corresponds to our theoretical model eq 33 with $[b/(|\tau|^3 l_B)]^{1/2} = 0.4$. The dashed line corresponds to Manning's model. The dotted (violet) line includes additional counterion condensation outside of the permeable globule. We note that this effect is a rather weak correction to the predictions of eq 33. It is discussed in detail in section V.

The proportionality constant in eq 30 was calculated by neglecting the first derivative term $(1/x)(du/dx)$ in eq 17, as explained in the context of eq 27, and solving the effective one-dimensional problem. Figure 3 shows that there is a very good agreement between the exact results and the analytical approximation in the limit $\tilde{Z}_g \gg 1$ ($\xi \ll x_g$). We also see that for a wide range of A values, our analytical theory gives a good numerical approximation for P as far as $P \lesssim 0.4$. For example, for $A = 500$, the relative error of our approximation is below 20% in this region. The exact numerical results were obtained using the method described in ref 25. As a guide to the eye, we have marked the parameter range explored in the experiments of W. Essafi et al. with a black arrow on Figure 3. This range was obtained from the experimental data as the ratio f_{eff}/f and is well within the range of validity of eq 31.

IV. The Effective Charge of a Hydrophobic Polyelectrolyte

In the regime explored experimentally by W. Essafi et al.,[22] the value of the dimensionless parameter A can be estimated as follows. For $|\tau| \simeq 1$, monomer concentration $C = 0.1$ mol L^{-1}, and the bond length in the polymer $b = 0.25$ nm, the expected value of $A \simeq |\tau|/(Cb^3)$ is $A \simeq 10^3 \gg 1$. The value of x_g depends on both the chemical and effective charge fraction, f and f_{eff}, as

$$x_g = \frac{R_g}{\lambda_D} \simeq \frac{|\tau|^{1/2}}{A^{1/2}}\left(\frac{l_B}{b}\right)^{1/6}\frac{f^{1/2}}{f_{eff}^{2/3}} \qquad (32)$$

Using eqs 22, 30, and 32, the effective charge fraction f_{eff} is found to be

$$f_{eff} \simeq \sqrt{\frac{b}{|\tau|^3 l_B}} f^{3/2} \qquad (33)$$

This result predicts that the effective charge fraction f_{eff} is proportional to $f^{3/2}$. We note that in this regime, the effective charge does not depend on the average monomer concentration C and depends only on intrinsic properties of the polymer. The scaling law of eq 33 and the experimental data of Figure 4 of ref 22 are shown in Figure 4. As one can see, there is a very good agreement between the predicted behavior and the experimental data. We stress that only one free coefficient of order 1 has been used to adjust the data. Thus, our theory can explain the origin of the difference between the effective charge predicted by the Manning law recalled in Figure 4 and that observed in experiments. Furthermore, using eqs 3, 7, and 33, the globule radius R_g and the number of monomers inside of the globule N_g are found to be $R_g \propto |\tau|b/f$ and $N_g \propto |\tau|^4/f^3$. Assuming that $|\tau| \sim 1$ and f varies in the range (0.2, 1), the above estimation for R_g allows to one convert $\tilde{Z}_g$ into Z_g. The experimentally relevant range shown on the x axis in Figure 3 is $\tilde{Z}_g \in (25, 225)$, which corresponds to Z_g in the range of $(8, 225)$.[36]

It is important to mention that in the experiments of ref 22, only samples with a relatively high chemical charge fraction of $f \geq 0.3$ were prepared, thereby limiting the range where our theory can be checked. This is related to the difficulty to stabilize solutions of hydrophobic polyelectrolytes with low chemical charge because the polyelectrolytes can form a macroscopic phase that is not soluble in the solvent. We expect that the formation of a macroscopic phase can occur if the number of monomers inside of a globule N_g becomes larger than the polymerization degree of the polymer N. In this case, the polymer chains must stick together to form globules of size $N_g \approx |\tau|^4/f^3 > N$, which may lead to form an entangled polymer network that is not soluble in the solvent anymore. More detailed theoretical studies are needed for this problem. We note that a detailed analysis of the possible phases and their stability range was performed in ref 28. As mentioned above, the dimensionless factors are on order 1, and if we set $N = 1000$, this condition for phase separation reads $f_{eff} < 1/(N)^{1/2} \simeq 0.03$. This result is in a reasonable agreement with the results displayed in Figure 4. It is worth mentioning that in the experiments, no point could be obtained below this limit. We also emphasize that in our theory, when a stable pearl necklace structure forms, the effective charge depends on N_g and not on polymerization degree N. This property has been verified in the experiment, where N has been varied from $N = 410$ to 2400 without apparent change of the measured values of f_{eff}.

V. Discussion

In the above treatment, we have assumed that the polyelectrolyte chain in a dilute regime forms a necklace structure in the solvent. Liao et al.[29] have studied the necklace formation in polyelectrolyte solutions using both theory and molecular dynamics simulations. They have shown that partially charged chains form necklace-like structures of globules and strings in

dilute solutions. For the dilute regime, the phase diagram of hydrophobic polyelectrolytes was obtained in ref 29. It has been shown that when the effective charge of the chain is larger than a threshold $[b|\tau|/(l_B N)]^{1/2}$, the necklace structure is the dominant feature of the polyelectrolytes in a bad solvent. Using eq 33 and the mentioned criterion, we find that for chains consisting of more than $1/(|\tau|^2 f^3)$ monomers, the necklace structure is formed in the system. For the experimental condition explained in ref 22, $|\tau| \simeq 1$ and $f > 0.2$ gives $1/(|\tau|^2 f^3) \simeq 150$. All of the chains that have been used in the experiment[22] have more than 410 monomers on a chain, which means that our model considering the necklace structure for the hydrophobic polyelectrolyte in the solution is reasonable. We note that our scaling approach does not allow one to predict accurately the phase diagram of the polyelectrolyte chains. A consistent minimization of the free energy would require one to properly account for the logarithmic dependence of the counterion entropic and electrostatic energy as a function of the pearl radius.[30] The origin of such logarithmic terms can be seen by estimating the entropy of the counterions since the condensed counterions explore only a phase volume of R_g^3 out of the total volume. In our analysis, this dependence is ignored because the available phase volume is limited to the size of the Wigner–Seitz cell in a periodic system. Furthermore, the correlation-induced effects like the nonmonotonic dependence of the solution osmotic coefficient on the polymer concentration have been observed in computer simulation analysis,[29] which cannot be described in our model.

As we explained before, eq 33 is based on the validity of eq 30. It is justified provided that $P \ll 1$; our numerical calculations suggest that reasonable agreement is already achieved for $P \lesssim 0.4$ for the experimental value of $A \simeq 10^3$. For the parameters used in Figure 4, the mentioned criterion is always satisfied. Furthermore, by placing the pearls inside of neutral Wigner–Seitz cells, we have ignored the effect of the interaction between neighboring pearls on the counterion distribution. However the sharp decrease of the counterion concentration on the boundary of the globule (see Figure 2) suggests that these interactions should not affect significantly the counterion distribution. We have also ignored the effect of the ions along the strings that connect adjacent pearls. This assumption can be checked by estimating the fraction s of the charged monomers present inside of the pearls. It can be shown that

$$s \simeq \frac{1}{1 + f_{\text{eff}} \sqrt{\dfrac{l_B}{|\tau|^3 b}}} \simeq \frac{1}{1 + f_{\text{eff}}} \tag{34}$$

where we have assumed that both the parameter $(l_B/|\tau|^3 b)^{1/2}$ and intermediate scaling constants are of order 1. These assumptions are consistent with the parameters used in Figure 4. Our theory holds as long as $s \simeq 1$; that is when the effective charge f_{eff} is small. While this is clearly the case in the range of small chemical charge f, the contribution of the strings may become important when $f \simeq 1$. Physically, we expect that around the strings, the counterions will follow the usual Manning condensation behavior. Therefore, the effect of the strings will be mainly to keep the effective charge f_{eff} below the Manning limit b/l_B. In Figure 4, the effective charge reaches this limit only at $f \simeq 1$; as a result, the effect of the strings is not visible, and our prediction holds even up to $f \simeq 1$.

Finally, we have not taken into account additional counterion condensation outside of the permeable globule. A popular criterion for counterion condensation in this setting was proposed
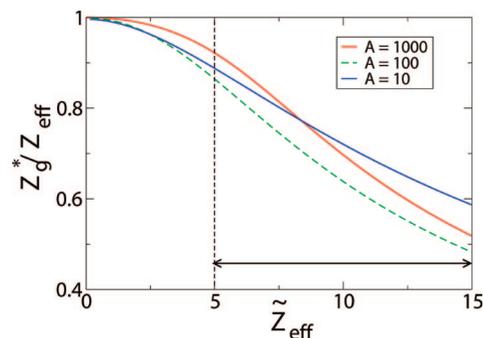

Figure 5. Ratio between the Alexander charge of the globule Z_g^* and the total charge inside of the globule $Z_{\text{eff}} = P Z_g$ as a function of $\tilde{Z}_{\text{eff}} = Z_{\text{eff}} l_B / R_g$ for different values of the inverse volume fraction A. ($A \approx 10^3$ in the experimental conditions.) The black arrow indicates the parameter range explored experimentally by Essafi et al. estimated from eq 35.

by Alexander et al.[31] The renormalized charge Z_g^* of an impermeable globule of internal charge Z_{eff} is determined from a linearization of the PB equation that ensures the best possible matching between the exact and linearized solutions at the boundary of the Wigner–Seitz cell. In our case, the globule is permeable, and Z_{eff} is smaller than the charge of the co-ions inside of the globule and is given by $Z_{\text{eff}} = P Z_g$. (We remind that P stands for the counterion fraction outside of the globule.) The dependence of the ratio Z_g^*/Z_{eff} on the system parameters is governed by the dimensionless parameter $\tilde{Z}_{\text{eff}} = Z_{\text{eff}} l_B / R_g$, where R_g is the globule radius.[31,32] This parameter can be estimated as follows for the case of our permeable pearl model: $\tilde{Z}_{\text{eff}} = P Z_g l_B / R_g = P_g$. Inserting the expression of P from eq 31 leads to

$$\tilde{Z}_{\text{eff}} = \sqrt{\frac{6 \tilde{Z}_g}{e}} = \frac{6}{eP} \tag{35}$$

Since the range explored by P is $(0.15, 0.4)$, the above expression allows us to conclude that $\tilde{Z}_{\text{eff}} \in (5, 15)$. We have calculated the ratio Z^*/Z_{eff} in this parameter range using the semianalytical method proposed in ref 33 and our numerical procedure. The results obtained are presented in Figure 5 and do not show significant renormalization in our regime. By combining the numerical results for inverse volume fraction $A = 1000$ and the analytical results from eq 33, we can calculate the effective charge of the globules including condensation outside of the globule. Indeed, the renormalized Alexander charge of the globule is given by $Z^*/Z_{\text{eff}} P f$, where the product $P f$ gives, as usual, the charge inside of the globule. The behavior of the Alexander charge for this problem is shown in Figure 4 on the dotted line, which is the continuous line of equation $f_{\text{eff}} = P f$ scaled down by a factor Z^*/Z_{eff}. The comparison between these two curves confirms that eq 33 is a very good approximation for the effective charge of the globule. For example, in the region explored experimentally, the difference between these two curves lies within the experimental uncertainty range.

It is interesting to compare our results with the results of Dobrynin and Rubinstein.[17] These authors considered for the first time the problem of counterion condensation around an hydrophobic polyelectrolyte using a two-state model. They determined the fraction P by using trial counterion densities of the form $n(r) = (1 - P) n_{\text{av}} R^3 / R_g^3$ inside of the globule (for $r < R_g$) and $n(r) = P n_{\text{av}} R^3 / R^3 - R_g^3$ in the outer region. This family of density is parametrized only by the parameter P. Therefore, by minimizing the counterion free-energy density functional on

On the Effective Charge of Hydrophobic Polyelectrolytes

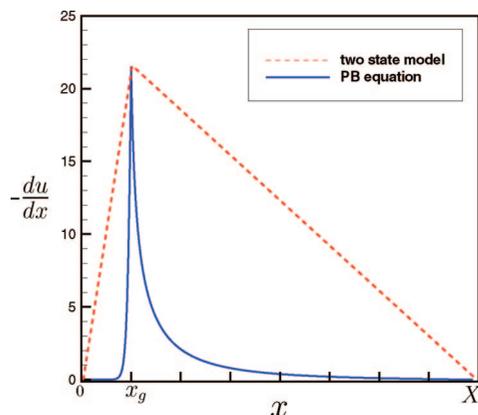*J. Phys. Chem. B, Vol. 113, No. 12, 2009* **3749**

Figure 6. Typical behavior of the dimensionless electric field $-du/dx$ using either the two-state model (dashed line) or our PB model (solid line). The solid line corresponds to $x_g = 1$ and $A = 500$.

this trial set, they could deduce an expression of P as a function of the system parameters.[34] However for reasonable values of $|\tau|(b/l_B)^{1/3} \simeq 1$ and for the experimental value of $A \simeq 10^3$, the value of f_{eff} predicted from the equations of ref 17 is very close to f in most of the parameter range, in contradiction with the experimental results of ref 22. We attribute the difference between our model and the results of ref 17 to the two-state model used to estimate the fraction of dissociated counterions P. Indeed, in the two-state model, the charge density is constant in the two regions inside and outside of the globule. The Poisson equation then implies that in the two-state approximation, the graph of the electric field ($-du/dx$ in our dimensionless units) as a function of x has a typical angle shape for all values of P, as illustrated in Figure 6. In this figure, we have also compared this approximation to the exact numerical behavior of $-du/dx$ for the typical parameters $A = 500$ and $x_g = 1$. Since the charged monomers at the center of the globule are neutralized by the counterions, the true electric field distribution takes the form of a narrow peak centered at x_g. Because of its reduced family of trial functions, the two-state model cannot reproduce the true behavior of the electric field. However, the determination of the effective charge requires an accurate knowledge of the electric field in the whole cell. Therefore, we believe that the two-state model is not accurate enough for the determination of the effective charge. Indeed, it was shown in ref 35 that at least a three-state model is necessary in the case of a permeable droplet.

VI. Conclusions

In conclusion, we have developed a theory of counterion condensation around hydrophobic polyelectrolytes. Our theory is based on the pearl necklace model for the polyelectrolyte backbone. We assumed that the pearls are permeable to the counterions and use analytic results on the Poisson−Boltzmann equation to establish the fraction of counterions condensed inside of the pearls. It allows us to establish a power law dependence of the effective charge f_{eff} on the chemical charge f as $f_{eff} \propto f^{3/2}$. This prediction is in very good agreement with recent experimental results by W. Essafi et al.[22] and explains the large deviation from the Manning law observed in these experiments.

While our main results concern the effective charge of hydrophobic polyelectrolytes, the scaling laws that we derived may also apply to other areas of physics and chemistry where the Poisson−Boltzmann equation plays an important role.

References and Notes

(1) Manning, G. S. *J. Chem. Phys.* **1969**, *51*, 924.
(2) Oosawa, F. *Polyelectrolytes*; Marcel Dekker: New York, 1971.
(3) Kantor, Y.; Li, H.; Kardar, M. *Phys. Rev. Lett.* **1992**, *69*, 61.
(4) Barrat, J.-L.; Joanny, J.-F. *Adv. Polym. Sci.* **1996**, *94*, 1.
(5) Holm, C.; Joanny, J.-F.; Kremer, K.; Netz, R. R.; Reineker, P.; Seidel, C.; Vilgis, T. A.; Winkler, R. G. *Adv. Polym. Sci.* **2004**, *166*, 67.
(6) Bloomfield, V. A.; Crothers, D. M.; Tinoco, I. *Nucleic Acids Structures, Properties and Functions*; University Science Books: Sausalito, CA, 2000.
(7) Philif, J. R.; Wooding, R. A. *J. Chem. Phys.* **1970**, *52*, 953.
(8) O'Shaughnessy, B.; Yang, Q. *Phys. Rev. Lett.* **2005**, *94*, 048302.
(9) Trizac, E.; Téllez, G. *Phys. Rev. Lett.* **2006**, *96*, 038302.
(10) Gonzalez-Mozuelos, P.; Olvera de la Cruz, M. *J. Chem. Phys.* **1995**, *103*, 22.
(11) (a) Naji, A.; Netz, R. R. *Phys. Rev. Lett.* **2005**, *95*, 185703. (b) Naji, A.; Netz, R. R. *Phys. Rev. E* **2006**, *73*, 056105.
(12) Alberts, B.; Bray, D.; Johnson, A.; Lewis, J.; Raff, M.; Roberts, K.; Walter, P. *Essential Cell Biology*; Garland Publishing: New York, 1998.
(13) Dobrynin, A. V.; Rubinstein, M.; Obukhov, S. P. *Macromolecules* **1996**, *29*, 2974.
(14) Raphael, E.; Joanny, J.-F. *Europhys. Lett.* **1990**, *13*, 623.
(15) Higgs, P. G.; Raphael, E. *J. Phys. I (France)* **1991**, *1*, 1.
(16) Carbajal-Tinoco, M. D.; Willliams, C. E. *Europhys. Lett.* **2000**, *52*, 284.
(17) Dobrynin, A. V.; Rubinstein, M. *Macromolecules* **2001**, *34*, 1964.
(18) Lee, M.-J.; Green, M. M.; Mikes, F.; Morawetz, H. *Macromolecules* **2002**, *35*, 4216.
(19) Kyriy, A.; Gorodyska, G.; Minko, S.; Jaeger, W.; Stepanek, P.; Stamm, M. *J. Am. Chem. Soc.* **2002**, *124*, 13454.
(20) Limbach, H. J.; Holm, C. *J. Phys. Chem. B* **2003**, *107*, 8041.
(21) Dobrynin, A. V.; Rubinstein, M. *Prog. Polym. Sci.* **2005**, *30*, 1049.
(22) Essafi, W.; Lafuma, F.; Baigl, D.; Williams, C. E. *Europhys. Lett.* **2005**, *71*, 938.
(23) Rayleigh, L. *Philos. Mag.* **1882**, *14*, 184.
(24) Baigl, D.; Ober, R.; Qu, D.; Fery, A.; Williams, C. E. *Europhys. Lett.* **2003**, *62*, 588.
(25) Wall, F. T.; Berkowitz, J. *J. Chem. Phys.* **1957**, *26*, 114.
(26) Belloni, L. *Colloids Surf. A* **1998**, *227*, 140.
(27) Trizac, E. *Phys. Rev. E* **2000**, *62*, R1465.
(28) Schiessel, H.; Pincus, P. *Macromolecules* **1998**, *31*, 7953.
(29) Liao, Q.; Dobrynin, A. V.; Rubinstein, M. *Macromolecules* **2006**, *39*, 1920.
(30) Dobrynin, A. V.; Rubinstein, M. *Macromolecules* **1999**, *32*, 915.
(31) Alexander, S.; Chaikin, P. M.; Grant, P.; Morales, G. J.; Pincus, P.; Hone, D. *J. Chem. Phys.* **1984**, *80*, 5776.
(32) Belloni, L.; Drifford, M.; Turq, P. *Chem. Phys.* **1984**, *83*, 147.
(33) Trizac, E.; Bocquet, L.; Aubouy, M.; von Grunberg, H. H. *Langmuir* **2003**, *19*, 4027.
(34) The final result is given in eq 21 of ref 17, where $P = x$.
(35) Deserno, M. *Eur. Phys. J. E* **2001**, *6*, 163.
(36) At the scaling level, we obtain $Z_g \propto 1/f^2$, which therefore spans an interval of amplitude 25, when f varies between 0.2 and 1, to be compared with $225/8 \simeq 28$. On the other hand, as far as $\tilde{Z}_g$ is concerned, we obtain an amplitude of $225/25 = 9$, whereas at scaling level, $\tilde{Z}_g \propto 1/f$, which corresponds to an amplitude factor of 5. Such comparisons provide tests for the self-consistency of our model, which is therefore qualiatively trustworthy but cannot achieve quantitative accuracy.